Mass Detectability in Dedicated Breast CT: A Simulation Study with the Application of Volume Noise Removal

Jessie Q. Xia, *Member, IEEE* and Joseph Y. Lo

***Abstract*—Dedicated breast Computed Tomography (CT) is an emerging new technique for breast cancer imaging. Breast CT data can be acquired at a dose level as low as the conventional two-view mammography. Since the dose is equally split into hundreds of projection views, each projection image contains non-ignorable quantum noise. This study is aimed at investigating how volume noise removal affects the mass detectability in breast CT. A Partial Diffusion Equation (PDE) based denoising technique was applied before the reconstruction of either a simulated breast volume embedded with a contrast-detail mass phantom or a real human subject breast CT volume embedded with a simulated spherical mass. By applying a mathematical observer, it is found that the PDE volume noise removal technique improves the mass detectability in breast CT in a statistically significant sense.**

***Index Terms*—breast cancer, tomography, noise, breast CT, lesion detection, observer study**

I. Introduction

The advance of flat panel detector technology made it possible to develop some three dimensional breast cancer imaging techniques, such as breast tomosynthesis [1] and dedicated breast CT [2]. Breast tomosynthesis acquires high-resolution projection images over a limited angle range. Its tomographic reconstruction is complicated by incomplete sampling and therefore is the focus of many research endeavors [3-6]. Intrinsically, reconstructed breast tomosynthesis volumes have high within-plane resolution and low cross-plane resolution. By contrast, dedicated breast CT acquires projection images over the full 360-degree angle span; whose tomographic reconstruction is conventional and can generate isotropic resolution both within plane and cross-plane. Due to the practical consideration, the flat-panel detector in breast CT system has lower spatial resolution than the one used in breast tomosynthesis system. Thus, the resolution in the reconstructed volume of breast CT is in-between the within-plane and cross-plane resolutions of breast tomosynthesis volumes.

Another image quality metric is noise level. Currently, dedicated breast CT techniques use the same dose as the one of conventional two-view mammography [7], which is split among hundreds of projection images. Due to the Poisson process of the projection views, the quantum noise is higher than the noise on mammograms. These noisy projection views are then reconstructed by using a reconstruction algorithm. The noise level in the reconstructed volume is heavily influenced by the noisiest projection view. In a separate study [8], we found that applying a noise removal module before reconstruction is much better than applying after reconstruction.

The motivation of the work presented in this paper is to investigate the effectiveness of a noise removal module in terms of mass detectability in breast CT. Consistent with our previous paper [8], we will use the Partial Diffusion Equation (PDE) based denoising technique applied on the line integral projection images.

II. Methods

A. Dedicated Breast CT System

A dedicated breast CT system is set up differently from the conventional CT system. Rather than illuminating the whole torso, it only illuminates a breast of the patient. Fig. 1 is an illustration of the major components of a typical breast CT system. The lead-shielded bed on which the patient lies prone was not shown in this illustration. The x-ray tube and the vertically standing flat panel detector rotate concurrently for a span of 360 degrees.

B. Datasets and Mass Simulation

There are two types of breast CT data used in this study: the ones acquired virtually for a simulated breast with simulated contrast detail phantoms in the middle of the breast; and the human-subject breast CT data from Dr. Boone's lab at University of California Davis.

Fig. 2 shows the cross-section of the simulated breast with contrast detail phantoms. Each of the five 4x4 arrays in contrast detail phantoms has masses with sizes varying vertically (6, 5, 4 and 3 mm) and contrasts varying horizontally (15%, 10%, 5% and 3%). Square regions

Manuscript received on May 4, 2008. This work was supported in part by NIH grant (R01 CA 94236 and R01 CA 112437) and the U.S. Army Breast Cancer Research Program (W81XWH-05-1-0278). We thank Professor John Boone's group in UC Davis for providing us with the breast CT datasets of human subjects. J.Q. Xia also thanks the National Institute of Statistical Sciences for supporting her to the conference.

J. Q. Xia was with the Department of Biomedical Engineering and the DAILabs of the Department of Radiology, Duke University, Durham, NC, 27710 USA. She is now with the National Institute of Statistical Sciences, RTP, NC 27709 USA (phone: 919-685-9313, email: xq8@niss.org).

J. Y. Lo is with the Department of Biomedical Engineering and the DAILabs of the Department of Radiology, Duke University, Durham, NC, 27710 USA (email: joseph.lo@ duke.edu).

containing all 80 masses form the 2D ROIs for numerical observer study.

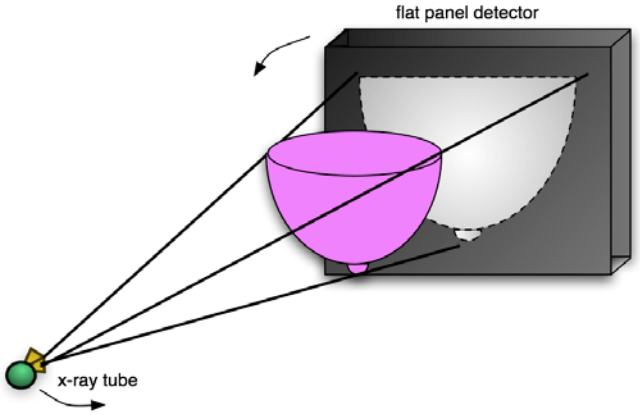

Fig. 1. In a dedicated breast CT system, the x-ray tube and flat-panel detector rotate simultaneously around the breast.

As the 20 human subject datasets used for the breast mass detectability study were prospectively collected cases, the ground truth of their volumes is unknown. In present study, we will assume that there is no lesion in the volumes. And all the lesions of interest will be simulated.

The procedure of simulating a mass in human subject breast CT data is as follows:

Step1: For a given human subject dataset, the reconstructed volume is used as the reference. The locations of 10 masses that will be embedded into the volume are randomly chosen.

Step2: Spherical masses with fixed size and contrast are put at the locations selected in Step 1, and projected onto a virtual 100% Detective Quantum Efficiency (DQE) detector using a virtual monochromatic cone-beam projector, which has the same system geometry, projection angles and reconstruction parameters as the individual human subject dataset. These projection images of masses will be added to the original projection images of human subjects to get the synthetic projection sets.

Step3: The synthetic projection sets either go through a denoising module followed by filtered back projection (FBP) reconstruction or directly go for FBP reconstruction.

Step4: The three-dimensional region of interest (ROIs) can then be retrieved from the reconstructed volumes. In the present study, instead of using 3D ROIs, only coronal region of interest containing the center of masses (i.e., 2D ROIs) are retrieved for numerical observer study.

Using the 80 ROIs (each of which contains a mass in the contrast-detail phantom) in the simulated breast volume, a PDE denoising technique was optimized. This technique was then applied to the human subject ROI dataset, which is comprised of a total of 400 ROIs, 200 with and 200 without simulated masses.

C. Volume Noise Removal

The PDE_{tomo} technique [8] for volume noise removal in breast CT is used in this study. Details of the technique can be found in the reference. A brief description of the technique is as follows.

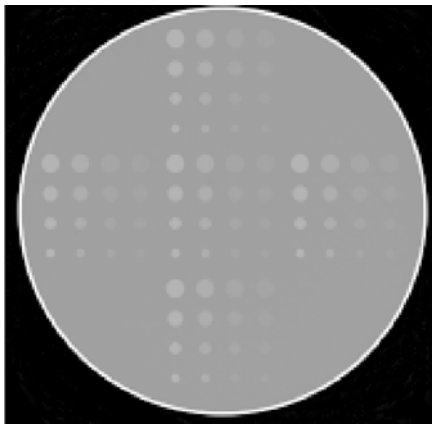

Fig. 2. Coronal view of a simulated breast embedded with a contrast-detail mass phantom.

The image to be denoised is denoted as *I*. A nonlinear partial diffusion equation on *I* will be:

$$\frac{\partial I}{\partial t} = \nabla \cdot (p(|\nabla (G_\sigma \otimes I)|)\nabla I), \qquad (1)$$

where ∇I is the gradient of the image *I* and $\nabla \cdot (*)$ is the divergence operator on image *I* over the spatial variables. By carefully selecting the appropriate *p(*)*, the diffusivity function, the image can be processed in such a way that not only noise is reduced but also the details in the image will be preserved. To bound the gradient values in the presence of noise, a Gaussian kernel G_σ with the standard deviation of sigma σ is convoluted with the image before gradients are computed as Catte *et al* [9] suggested.

In this study, we chose a diffusivity function with the form of

$$p(d) = e^{-\frac{d^2}{\delta^2}}, \qquad (2)$$

where delta δ is a user-specified parameter. The parameter δ acts like a cut-off value; image regions with gradient norm below δ will have more noise removed while regions with a higher gradient norm will stay sharp. We used a spatially adaptive type of the parameter δ as:

$$\delta_{ij} = \delta_0 \cdot \sqrt{\frac{1}{\frac{1}{M}\sum_{c \in N(i,j)} e^{l_c}}}, \qquad (3)$$

where *M* equals to 4, and *N (i, j)* is the four closest neighbors around pixel (i, j) of image *I*.

Equation (1) can be discretized by the finite difference approach using the first-order neighborhood system. Each pixel has four neighbors: the north, south, west and east neighbor pixels. Assuming $\Delta x = \Delta y = 1$ in the two-dimensional case, the discretized version of (1) is

$$\frac{I_{(i,j)}^{<t+1>} - I_{(i,j)}^{<t>}}{\Delta t} = p_{(i-1,j)} \cdot \nabla_{(i-1,j)} I^{<t>} + p_{(i+1,j)} \cdot \nabla_{(i+1,j)} I^{<t>} \quad , \quad (4)$$
$$+ p_{(i,j-1)} \cdot \nabla_{(i,j-1)} I^{<t>} + p_{(i,j+1)} \cdot \nabla_{(i,j+1)} I^{<t>}$$

where <t> and <t+1> represent the iteration step t and t+1 respectively; Δt is the discretized time step; $p_{(..)}$'s are diffusivity function values at the neighboring pixels of location (i,j); and $\nabla(.,.)I$ is a notation for the difference between $I_{(\cdot,\cdot)}$and $I_{(i,j)}$. The parameters used in this study are: Δt=0.1, σ=1, δ_0=0.03, and the number of iterations = 10.

D. Numerical Observers

D.1. Ideal Observer

The task of an observer is to detect these masses from background tissues. It can also be formulated as the following hypothesis testing:

$$H_0 : x = n$$
$$H_1 : x = n + s \quad , \qquad (5)$$

where n and s represent respectively the noise and the signal (in our application, it refers to the existence of a mass).

The null hypothesis represents the mass absent case, whereas the alternative hypothesis represents the mass present case. If treated as signal known exactly (SKE) case, according to signal detection theory [10], the optimal detector is a likelihood ratio detector. Assuming the background noise n follows a Gaussian distribution with a covariance matrix of Σ, the log likelihood ratio has the following form:

$$\ln(\lambda(x)) = s^T \Sigma^{-1} x \quad . \qquad (6)$$

If the background noise follows independent and identical distributed (I.I.D.) Gaussian, i.e., the covariance matrix Σ is an identity matrix, then (6) can be further simplified to:

$$\ln(\lambda(x)) = s^T x / \sigma^2 \quad . \qquad (7)$$

This is the ideal observer. Usually real breast tissue background does not satisfy the I.I.D. condition, so the ideal observer shown in (7) will perform sub-optimally on the real breast tissue background case.

D.2. Laguerre-Gauss Channelized Hotelling Observer (LG-CHO)

When the covariance matrix Σ is not an identity matrix, the likelihood ratio observer shown in (6) is equivalent to a Hotelling observer [11]. The estimation of the covariance matrix Σ requires a large number of training cases, which is presently not available in breast CT. Alternatively, Laguerre-Gauss channelized Hotelling observer (LG-CHO) [11, 12] can be used for this purpose.

The nth order Laguerre function has the following form:

$$L_n(x) = \sum_{m=0}^{n} (-1)^m \binom{n}{m} \frac{x^m}{m!} . \qquad (8)$$

The LG-CHO has n^{th} order template with the form of:

$$LG_n(r) = \exp(-\frac{\pi r^2}{a^2}) \cdot L_m(\frac{2\pi r^2}{a^2}), \qquad (9)$$

where *a* is a free parameter proportional to the standard deviation of the Gaussian kernel through

$$a = \sqrt{2\pi}\sigma . \qquad (10)$$

D.3. CNR Observer

Traditionally, one would like to use Rose model of statistical detection for a simple lesion detectability study based on x-ray projection images. However Rose model does not directly apply to the breast CT reconstructed slices in this study since the physical measurement on these reconstructed slices is linear attenuation coefficients. Instead, the contrast to noise ratio (CNR) for each ROI is calculated and used as the decision variable. Given the uncertainties associated with any model observer study, it is desirable to be able to compare all results against such a simple, well-understood technique.

E. ROC Analysis

The receiver operating characteristic (ROC) analysis is a comprehensive tool for performance measure of the numerical observers. Of the two axes on ROC plots, the horizontal axis represents one minus the specificity, or the False Positive Fraction (FPF), which equals to the ratio of the number of false positive responses to the number of actual negative cases. The vertical axis denotes sensitivity, or the True Positive Fraction (TPF), which equals to the ratio of number of true positive responses to the number of actual true cases. The FPF and the TPF both range from 0 to 1. A metric of ROC curve is the area under the curve (AUC). The larger AUC value, the better the performance is, while AUC of 0.5 corresponds to random guessing. The area can also be calculated via semi-parametric fitting resulting in an area index denoted as Az [13].

III. RESULTS

Results are presented hereafter for two cases: contrast detail phantoms in simulated breast CT background, and masses with fixed size and contrast in human subject background. First we present in Fig. 3 and Fig. 4 two sample ROIs for simulated masses embedded in the anatomical background. The top row showed the ROIs derived from the original dataset, whereas the bottom row showed the ROIs from the processed dataset with volume noise removal. The left column showed the ROIs without masses, while the right column showed the ROIs containing the simulated masses following Step1 to Step 4 in Methods section B.

A. Contrast Detail Phantom Results

CNR observer result is shown in Fig. 5 for the contrast detail phantom embedded in a uniform background.

In Fig. 5 (a), the histograms of CNR for original and PDE processed ROIs with and without simulated masses are plotted. It is obvious that PDE processed ROIs with simulated masses have higher CNR values than original ROIs with masses.

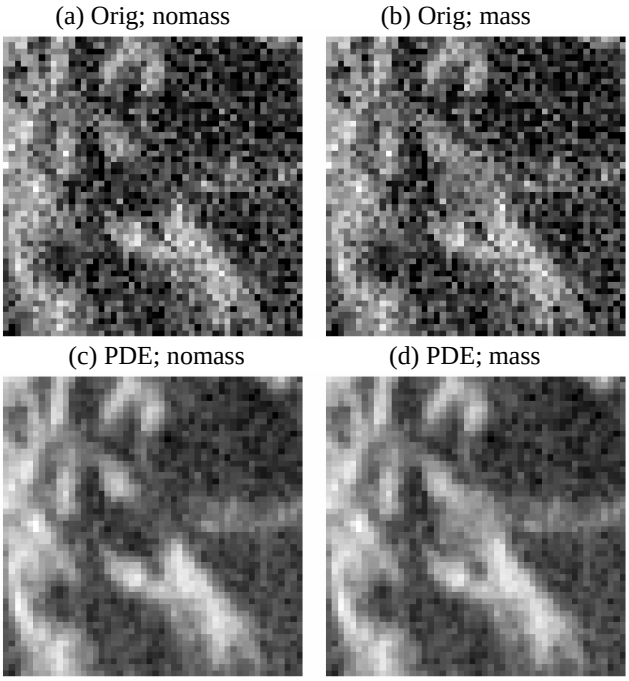

Fig. 3. Sample ROIs for simulated lesion of 5 mm in diameter and 3% in contrast: Original ROIs in (a) without mass and in (b) with a mass, and, PDE denoised ROIs in (c) without mass and in (d) with a mass.

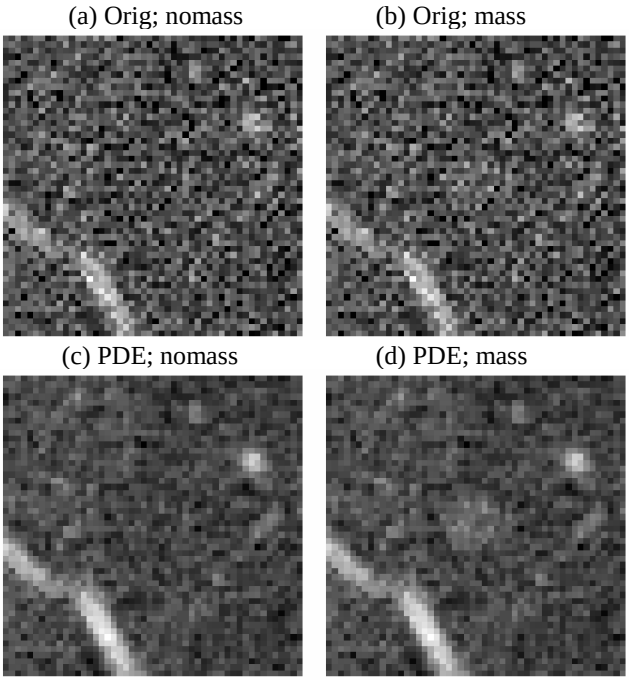

Fig. 4. Sample ROIs for simulated lesion of 4 mm in diameter and 2% in contrast: Original ROIs in (a) without mass and in (b) with a mass, and, PDE denoised ROIs in (c) without mass and in (d) with a mass.

The Az values were obtained using the software package ROCKIT (Charles Metz, University of Chicago). For original dataset, the Az is 0.933 ± 0.020; and for PDE processed dataset, the Az is 0.998 ± 0.005. The corresponding two-tailed p value is 0.0009, indicating that Az of PDE processed dataset is statistically higher than Az of the original dataset. The ROC curves are shown in Fig. 5 (b).

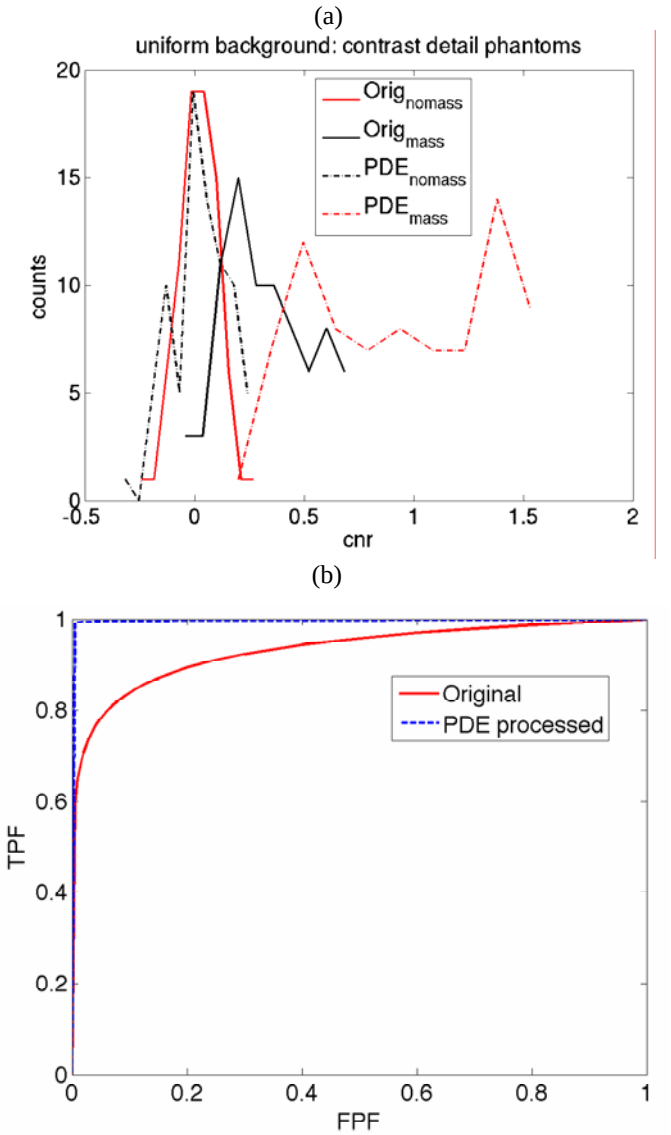

Fig. 5. CNR observer results for contrast detail phantoms embedded in a simulated uniform background. CNR histograms for original and PDE processed ROI databases are shown in (a) and the corresponding ROC curves are shown in (b). The Az value of the PDE processed dataset (0.998 ± 0.005) is statistically higher than the Az value of the original dataset (0.933 ± 0.020). The p value is less than 0.01.

B. Human Subject Background Results

The human subject background ROC analysis based on CNR observer is shown in Fig. 6 for simulated masses of 4 mm and 2%. The histograms of CNR for original and PDE processed datasets with and without simulated masses are shown in Fig. 6(a). The corresponding ROC curves are plotted in Fig. 6(b). The Az value of the PDE processed dataset (0.801 ± 0.022) is higher than the Az value of the original dataset (0.770 ± 0.023). The p value is less than 0.009, indicating that the difference is statistically significant.

(a)

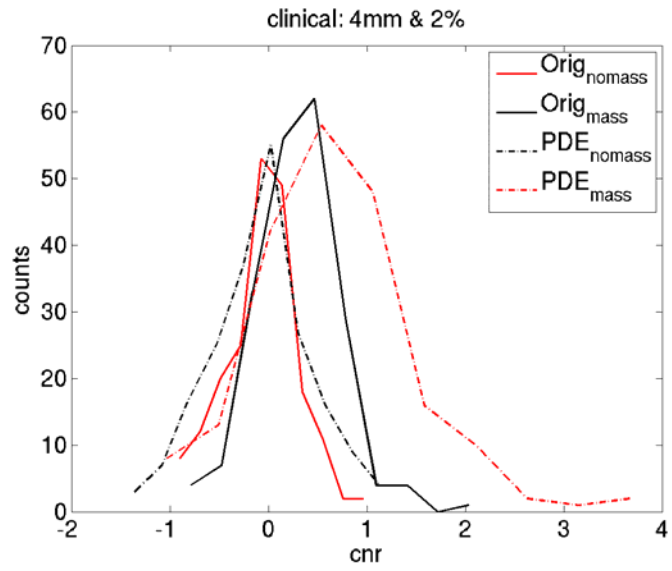

(b)

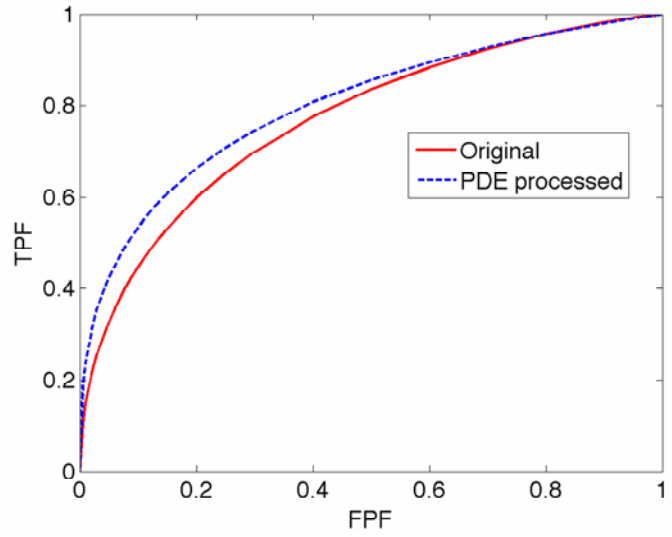

Fig. 6. CNR observer results for simulated lesions of 4mm and 2% embedded in real anatomical backgrounds. CNR histograms for original and PDE processed ROI databases are shown in (a) and the corresponding ROC curves are shown in (b). The Az value of the PDE processed dataset (0.801 ± 0.022) is statistically higher than the Az value of the original dataset (0.770 ± 0.023). The p value is less than 0.01.

AUC values of the three types of numerical observers using real anatomical background from breast CT are shown in Table I for lesions of 5 mm and 10%, 5 mm and 3%, and 4 mm and 2%, respectively. For all the cases, the CNR observer gives the highest AUC values, followed by 1st order LG template, and the ideal observer gives the lowest AUC values. For masses with 4 mm diameter and 2% contrast, the ROC performance of ideal observer reduces to the chance curve.

IV. Discussion

Some studies [14-18] have shown that numerical observers can be good candidates for lesion detection tasks.

As compared to human observers, numerical observers posses several advantages, such as higher repeatability, and better tolerance of tedious process of observer studies. In this study, detectability of simulated masses in both simulated breast CT background and the real anatomical background were investigated. CNR observers were used in both cases. In addition, a SKE ideal observer and n^{th} order LG-CHO observers were used for detecting the simulated masses in the anatomical background. As expected, SKE ideal observer worked sub-optimally whereas LG-CHO worked much better than SKE case. The CNR observer as a simple one worked the best, as is evident in Table I.

For the contrast detail phantom in a simulated uniform breast background, shown in Fig. 5, the initial AUC based on CNR observer is 0.933 ± 0.020. After PDE denoising, the AUC improves to 0.998 ± 0.005, which is close to the perfect performance. The improvement is statistically significant with two-tailed $p<0.001$.

With real anatomical backgrounds, masses with a single combination of size and contrast was embedded. And the resultant ROC curves are a function of both the mass size and contrast. It is very easy to detect large masses (e.g., 5 mm in diameter and 10% in contrast), whereas the detection task is extremely challenging for subtle masses (e.g., 4 mm in diameter and 2% in contrast). Using a CNR observer in the latter condition showed that PDE denoising provided statistically significant improvements in performance, as well as higher CNR values and better visual appearance.

There are some limitations in this study. First, the simulated masses are perfect spheres, which are rare in the real situation. A more realistic mass simulation may render more advantages toward evaluating nonlinear image processing techniques such as PDE_{tomo}. Second, the ROIs are two dimensional due to the limited number of human subject datasets available. In the future, when more human subject datasets are collected, three-dimensional ROIs can be used instead. Third, in this study, individual LG-CHO channels are used for ROC analysis. An ensemble LG-CHO is often used with the form:

Table I: Numerical observer AUC values for simulated masses in real anatomical background of breast CT.

Lesion		5mm & 10%	5mm & 3%	4mm & 2%
CNR Observer	Original	0.999	0.877	0.770
	PDE processed	0.997	0.883	0.801
LG-CHO Observer	Original	0.999	0.850	0.703
	PDE processed	0.999	0.853	0.702
Ideal Observer	Original	0.896	0.690	0.446
	PDE processed	0.904	0.700	0.443

$$w = \sum_{m=0}^{n} \alpha_m LG_m(r), \qquad (11)$$

where the parameters (α_1, α_2, α_3,….) are determined by Hotelling Observer.

A common problem shared by the observers is the tendency to perform too well due to the fixed, single type of lesion. Even for the subtlest lesions (masses with 4mm in diameter and 2% in contrast in this study) that were virtually impossible to see by the human eye, the observers routinely performed quite well with ROC areas around 0.7 to 0.8. As such, such mathematical observer performances should not be construed as what would be typical of clinical performance by radiologists. Instead, these studies offer valuable insight in terms of comparing one technique against another in a fair (or equally unfair) fashion. The best techniques from such a study may then be validated in human observer studies in the future. In summary, several numerical observers are used to analyze the mass detectability in breast CT using simulated uniform background and real anatomical background. With simulated uniform background and contrast detail phantoms, the PDE denoised datasets give the better results than the original datasets using CNR observer. The performances are similar when LG-CHO templates are used. With real anatomical background with fixed size lesion, PDE denoised images have higher detectability, higher CNR and better qualitative appearance.

V. Conclusion

This manuscript has presented the ROC study using simulated masses and mathematical observers. With either simulated background or the real anatomical breast CT background, volume noise removal of breast CT dataset improves significantly the detectability of masses.

References

[1] J. T. Dobbins, III and D. J. Godfrey, "Digital x-ray tomosynthesis: current state of the art and clinical potential," *Physics in Medicine and Biology*, vol. 48, pp. R65-R106, 2003.

[2] S. J. Glick, "Breast CT," *Annual Review of Biomedical Engineering*, vol. 9, pp. 501-526, 2007.

[3] T. Wu, R. H. Moore, E. A. Rafferty, and D. B. Kopans, "A Comparison of Reconstruction Algorithms for Breast Tomosynthesis," *Medical Physics*, vol. 31, pp. 2636-2647, 2004.

[4] G. Lauritsch and W. H. Harer, "A theoretical framework for filtered backprojection in tomosynthesis," *Proceedings of SPIE*, vol. 3338, pp. 1127-1137, 1998.

[5] T. Mertelmeier, J. Orman, W. Haerer, and M. K. Dudam, "A theoretical framework for filtered back-projection in tomosynthesis," *Proceedings of SPIE*, vol. 6142, pp. 6142F1-12, 2006.

[6] Y. Chen, J. Y. Lo, and J. T. Dobbins, 3rd, "Impulse response analysis for several digital tomosynthesis mammography reconstruction algorithms," *Proceedings of SPIE*, vol. 5745, pp. 541-549, 2005.

[7] J. M. Boone, "Performance Assessment of a Pendant-geometry CT Scanner for Breast Cancer Detection," *Proceedings of SPIE*, vol. 5745, pp. 319-323, 2005.

[8] J. Q. Xia, J. Y. Lo, K. Yang, C. E. Floyd Jr, and J. M. Boone, "Dedicated breast computed tomography: Volume image denoising via a partial-diffusion equation based technique," *Medical Physics*, vol. 35, pp. 1950-1958, 2008.

[9] F. Catte, P. L. Lions, J. M. Morel, and T. Coll, "Image Selective Smoothing and Edge-detection by Nonlinear Diffusion," *SIAM Journal on Numerical Analysis*, vol. 29, pp. 182-193, 1992.

[10] S. M. Kay, *Fundamentals of Statistical Signal Processing: Detection Theory*: Prentice Hall, 1998.

[11] H. H. Barrett, C. K. Abbey, and B. Gallas, "Stabilized estimates of Hotelling-observer detection performance in patient-structured noise," *Proceedings of SPIE*, vol. 3340, pp. 27-43, 1998.

[12] A. H. Baydush, D. M. Catarious, and C. E. Floyd, Jr, "Computer aided detection of masses in mammography using a Laguerre-Gauss channelized Hotelling observer," *Proceedings of SPIE*, vol. 5034, pp. 71-76, 2003.

[13] C. E. Metz, B. A. Herman, and J. H. Shen, "Maximum likelihood estimation of receiver operating characteristic (ROC) curves from continuously-distributed data," *Statistics in Medicine*, vol. 17, pp. 1033-1053, May 1998.

[14] H. H. Barrett, J. Yao, J. P. Rolland, and K. J. Myers, "Model Observers For Assessment of Image Quality," *Proceedings of the National Academy of Sciences of the United States of America*, vol. 90, pp. 9758-9765, 1993.

[15] M. P. Eckstein, C. K. Abbey, and J. S. Whiting, "Human vs. model observers in anatomic backgrounds," *Proceedings of SPIE* vol. 3340, pp. 16-26, 1998.

[16] M. P. Eckstein, C. K. Abbey, F. O. Bochud, J. L. Bartroff, and J. S. Whiting, "The effect of image compression in model and human performance," *Proceedings of IEEE*, vol. 3663, pp. 243-252, 1999.

[17] Y. Zhang, B. T. Pham, and M. P. Eckstein, "Task-based model/human observer evaluation of SPIHT wavelet compression with human visual system-based quantization," *Academic Radiology*, vol. 12, pp. 324-336, Mar 2005.

[18] J. Yao and H. H. Barrett, "Predicting human performance by a channelized hotelling observer model," *Proceedings of SPIE*, vol. 1768, pp. 161-168, 1992.